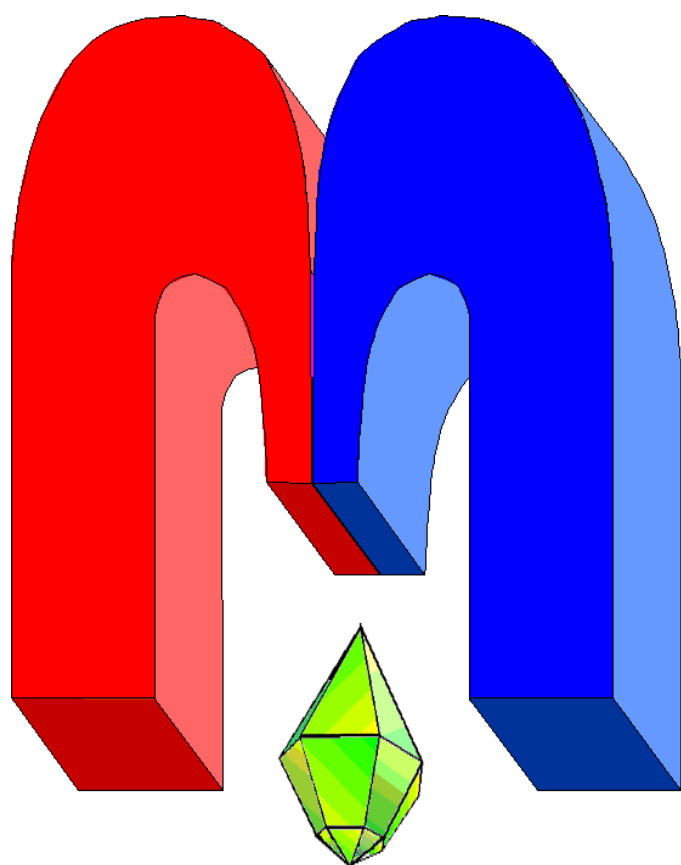


ISSN 2072-5981

doi: 10.26907/mrsej



***magnetic
Resonance
in Solids***

Electronic Journal

Volume 26

Issue 2

Article No 24208

1-10 pages

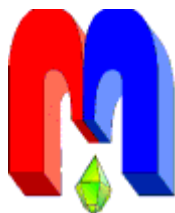
June, 6

2024

doi: 10.26907/mrsej-24208

<http://mrsej.kpfu.ru>

<https://mrsej.elpub.ru>



Established and published by Kazan University*
Endorsed by International Society of Magnetic Resonance (ISMAR)
Registered by Russian Federation Committee on Press (#015140),
August 2, 1996
First Issue appeared on July 25, 1997

© Kazan Federal University (KFU)†

"Magnetic Resonance in Solids. Electronic Journal" (MRSej) is a peer-reviewed, all electronic journal, publishing articles which meet the highest standards of scientific quality in the field of basic research of a magnetic resonance in solids and related phenomena.

Indexed and abstracted by
*Web of Science (ESCI, Clarivate Analytics, from 2015),
Scopus (Elsevier, from 2012), RusIndexSC (eLibrary, from 2006), Google Scholar,
DOAJ, ROAD, CyberLeninka (from 2006), SCImago Journal & Country Rank, etc.*

Editor-in-Chief

Boris **Kochelaev** (KFU, Kazan)

Honorary Editors

Jean **Jeener** (Universite Libre de
Bruxelles, Brussels)


Raymond **Orbach** (University of
California, Riverside)

Executive Editor

Yurii **Proshin** (KFU, Kazan)
mrsej@kpfu.ru



This work is licensed under a [Creative Commons Attribution-ShareAlike 4.0 International License](https://creativecommons.org/licenses/by-sa/4.0/).

 This is an open access journal which means that all content is freely available without charge to the user or his/her institution. This is in accordance with the [BOAI definition of open access](https://www.boai.ru/).

Technical Editors

Maxim **Avdeev** (KFU, Kazan)
Vadim **Tumanov** (KFU, Kazan)
FaiI **Siraev** (KFU, Kazan)

Editors

Vadim **Atsarkin** (Institute of Radio
Engineering and Electronics, Moscow)

Yurij **Bunkov** (CNRS, Grenoble)

Mikhail **Eremin** (KFU, Kazan)

David **Fushman** (University of
Maryland, College Park)

Hugo **Keller** (University of Zürich,
Zürich)

Yoshio **Kitaoka** (Osaka University,
Osaka)

Boris **Malkin** (KFU, Kazan)

Alexander **Shengelaya** (Tbilisi State
University, Tbilisi)

Jörg **Sichelschmidt** (Max Planck
Institute for Chemical Physics of
Solids, Dresden)

Haruhiko **Suzuki** (Kanazawa
University, Kanazawa)

Murat **Tagirov** (KFU, Kazan)

Dmitrii **Tayurskii** (KFU, Kazan)

Valentine **Zhikharev** (KNRTU,
Kazan)

Invited Editor of Special Issue[‡]: Eduard Baibekov (KFU, Kazan)

* Address: "Magnetic Resonance in Solids. Electronic Journal", Kazan Federal University; Kremlevskaya str., 18; Kazan 420008, Russia

† In Kazan University the Electron Paramagnetic Resonance (EPR) was discovered by Zavoisky E.K. in 1944.

‡ Dedicated to Professor Boris Z. Malkin on the occasion of his 85th birthday

Photoinduced EPR and ENDOR studies of the divacancies and nitrogen-vacancy defects in silicon carbide[†]

F.F. Murzakhanov¹, L.R. Latypova^{2,3*}, G.V. Mamin¹, M.A. Sadovnikova¹, H.J. von Bardeleben⁴, M.R. Gafurov¹

¹ Kazan Federal University, Kazan 420008, Russia

² School of Chemistry and Chemical Engineering, Harbin Institute of Technology, Harbin 150001, China

³ Zhengzhou Research Institute, Harbin Institute of Technology, Zhengzhou 450000, China

⁴ Sorbonne Université, Campus Pierre et Marie Curie, Institut des Nanosciences de Paris, Paris 75005, France

*E-mail: larisa.latypova@hit.edu.cn

(Received May 8, 2024; accepted May 30, 2024; published June 6, 2024)

Defects (color centers) in wide-gap semiconductors are considered as the basis for the realization of highly sensitive sensors, single-photon sources, and for the implementation of quantum technologies. Silicon carbide (SiC) crystal can serve as a reliable solid-state matrix for the range of high-spin (electron spin $S = 1$) color centers to become an alternative to the diamond with the widely-known nitrogen-vacancy (NV^-) centers. This paper reviews the electron paramagnetic resonance (EPR) and electron-nuclear double resonance (ENDOR) studies of the divacancies (VV) and negatively charged NV^- centers in different SiC polytypes. The main spin Hamiltonian components of non-equivalent spin defects in SiC are presented depending on their structural features (positions) and local environment: the zero-field splitting ($D \approx 1.3$ GHz), hyperfine ($A \approx 1.1$ MHz) and quadrupole ($P \approx 1.8$ MHz) interaction values. The luminescence spectrum of the color center in SiC ($\lambda = 1.1 - 1.25 \mu\text{m}$) in near-IR range is favorable for fiber-optic channels (O-band) and biological objects study, which brings these defects to a higher level of practical application.

PACS: 76.30.Mi, 76.30.-v, 76.70.Dx.

Keywords: silicon carbide, color centers, electron paramagnetic resonance, optical polarization, spin defects

1. Introduction

Semiconductor materials with point defects in their crystal lattice have been considered as systems for the potential implementation of quantum computing algorithms [1]. Vacancy-type defects (color centers) formed due to external influences can lead to changes in the optical properties of the material in the visible range [2]. The electron spin provides at least two stable states in an external strong magnetic field where further consideration of color centers as qubits implies a combination of magnetic, optical and charge properties to enable complex manipulations in quantum technologies by combining optical, microwave (MW) and radio frequency (RF) influences. The presence of a magnetic nuclear spin near the defect turns color centers into an even more attractive quantum object due to the formation of a multiqubit structure through electron-nuclear interaction and the possibility of creating quantum memory (registers) [1]. In this case, the electron density of color centers should be concentrated near the defect with minimal spin-orbit interaction to ensure the maximum possible values of phase coherence times [1,3]. Semiconductors are considered as optimal matrices for color centers primarily due to the wide band gap (≥ 3 eV) which prevents thermal transfer of defect charge to the conduction band,

[†]This paper is dedicated to Professor Boris Z. Malkin, who made a significant contribution to the field of magnetic radio spectroscopy in Kazan University, on the occasion of his 85th birthday.

thereby ensuring stability of the charge state. The second advantage is associated with the intracenter optical transition of color centers, which leads to the polarization of its electronic spin sublevels. Thus, color centers possessing optically polarizable electronic states in semiconductor materials are promising platforms for the implementation of quantum information technologies [4, 5].

Among the diverse studied materials, the most widely known and studied example of color centers is a nitrogen-vacancy defect (NV^-) center in the crystal lattice of a diamond, which is already actively used in quantum cryptography [6], quantum information networks [7] and as a quantum sensor with submicron spatial resolution [8, 9]. One noteworthy semiconductor material for quantum technology needs is silicon carbide (SiC). In these materials, a wide variety of electronic defects with triplet spin states ($S = 1$) and with long spin-spin relaxation times (phase coherence) have been discovered, which can be optically controlled (manipulated) [10–12]. The luminescence spectrum (in the range of $1.1 - 1.25 \mu\text{m}$ of known optically polarizable centers in SiC falls in the infrared (IR) range. In this case, zero-phonon lines fall into the transparency window of optical fibers (for use in telecommunication networks) and biological objects (for use as biosensors), and optical excitation can be carried out in a wide range of wavelengths (λ) from 280 nm to 1064 nm [13]. The technology for the synthesis of such crystals (with a small number of defects and inhomogeneities in the initial crystal matrix), which are wide-gap semiconductor materials with a covalent type of bond (sp^3 -hybridization), is well-developed. The SiC material has high radiation resistance and temperature stability, which allows the crystal to be exploited in extreme conditions (for use in space technology, operating at elevated temperatures and high pressures, etc.) [14]. Thus, it seems extremely interesting to search for and identify electronic configurations with an optically polarizable triplet state in the crystal lattice of silicon carbide.

The presence of electron spin in color centers allows the use of various techniques based on the electron paramagnetic resonance (EPR) to manipulate and read the electronic state of a defect. The use of various EPR spectroscopy techniques in combination with electron-nuclear double resonance (ENDOR) opens up the possibility of obtaining detailed information about the spin system, electron-nuclear interactions, electron density distribution and dynamic (relaxation) properties of the magnetic system [15–17], which is a necessary condition for considering and using color centers as elementary units in quantum technologies [18]. In this paper we review previous results of our EPR and ENDOR studies for various color centers in SiC crystals.

2. Materials and methods

2.1. Materials

The bulk crystal studied in this article was a N-doped ($2 \cdot 10^{17} \text{ cm}^{-3}$) n-type 4H-SiC obtained by a physical vapor transport (PVT) way where the source material sublimates and the vapor species diffuse and deposit onto the seed to form single N-doped SiC crystals. PVT growth techniques have proven to produce commercially usable SiC materials. Material has been irradiated by 15 MeV protons with a total dose of $1 \cdot 10^{16} \text{ cm}^{-2}$ in order to create Si vacancy centers. To form divacancies and $\text{V}_{\text{Si}}\text{-N}_{\text{C}}$ complexes by Si vacancy diffusion, the sample was annealed at $T = 1300^\circ\text{C}$. A typical 4H-SiC size was $0.8 \text{ mm} \times 0.4 \text{ mm} \times 0.2 \text{ mm}$.

2.2. Methods

The magnetic resonance experiments were carried out with a Bruker Elexsys E680 commercial spectrometer operating at $\nu_{\text{MW}} = 94 \text{ GHz}$ (W-band) in a pulsed mode. The photoinduced $\lambda = 532 \text{ nm}$ EPR spectra were recorded by detecting the amplitude of the primary electron spin

echo (ESE) as a function of the magnetic field sweep \mathbf{B} using a pulse sequence $\pi/2 - \tau - \pi - \tau - \text{ESE}$, where $\pi/2$ pulse duration is 40 ns and $\tau = 240$ ns. The relaxation times were measured with standard pulse sequences: the Hahn sequence for recording the phase coherence time T_M and the inversion-recovery sequence ($\pi - T + dT - \pi/2 - \tau - \pi - \tau - \text{ESE}$, where $T = 1.5 \mu\text{s}$ and $dT = 1 \mu\text{s}$) for recording the spin-lattice relaxation time T_1 . ENDOR spectra were obtained utilizing the Mims pulse sequence ($\pi_{\text{MW}} - \pi_{\text{RF}} - \pi_{\text{MW}}/2 - \tau - \pi_{\text{MW}} - \tau - \text{ESE}$) with a 150 kW RF generator, where $\pi_{\text{RF}} = 18 \mu\text{s}$. For the low temperature measurements, we used a continuous flow helium cryostat from Oxford Instruments. Laser sources with λ from 260 nm to 980 nm and an average output power from 10 mW to 200 mW were exploited for the photoinduced EPR measurements.

2.3. Structural features of color centers in silicon carbide

More than 250 SiC polytypes are known, few of which are thermodynamically stable, and five short-period polytypes (2H, 3C, 4H, 15R, and 6H) are considered to be the basic structures of SiC. The 3C, 4H (the defect configurations hh and kk , which have C_{3v} symmetry, are called axial configurations, since the defect axis is parallel to the c axis, and configurations kh and hk are off-axis (basal) configurations with C_{1h} symmetry) and 6H (three axial (hh , k_1k_1 , k_2k_2) and three off-axis or basal configurations (hk_1 , k_1k_2 , k_2h)) polytypes are perfect from the point of view of mechanical and physico-chemical properties, and the most technologically important [19].

Irradiation of different SiC polytypes with a flow of high-energy particles leads to the formation of stable vacancy centers, which can be isolated (silicon vacancy) or paired - divacancies (the nearest pair of silicon and carbon vacancies). These point defects can have completely different structures and significantly affect the optical and magnetic properties of the material. To understand the physical nature of the created color centers, it is necessary to carry out a number of spectroscopic studies. Divacancies $V_{\text{Si}}-V_{\text{C}}$ are common defects in semiconductors, consisting of adjacent isolated vacancies. For the first time, divacancies of various natures were detected by EPR in a heat-treated 6H-SiC crystal [20] and were later demonstrated to be common defects in SiC n -type semiconductors [21]. The positions of atoms in the SiC lattice are designated as hexagonal (h) and quasi-cubic (k), depending on whether the arrangement of the atom's nearest neighbors corresponds to hexagonal wurtzite or cubic zinc sulfide ZnS (zinc blende) structure. The defect forms one configuration in 3C (kk), four configurations in 4H (hh , kk , hk , kh) and six configurations in 6H (k_1k_2 , hh , k_2k_1 , k_2k_2 , k_1h , k_2h) polytypes. If the neighboring atom is on the axis, i.e. the symmetry axis of the defect is parallel to the c -axis of the crystal, the defect is called axial center with C_{3v} symmetry (direct equivalent symmetry to the NV^- in diamond). Otherwise, the point symmetry group of the defect is C_{1h} called the basal center.

3. Results

3.1. EPR spectroscopy

The photoinduced EPR signals are presented in Figure 1. The use of a source with $\lambda = 532$ nm leads to the appearance of an intense signal with the highest signal-to-noise ratio. In this case, a phase inversion of high-field lines is observed in the EPR spectrum (Figure 1a). While color centers are excited by other wavelengths, an EPR signal of lower intensity also appears; no phase inversion was observed (Figure 1b). Accordingly, in all experiments in this work, a laser with $\lambda = 532$ nm (green color) was used. The doublet shape of the spectrum is due to the presence of a triplet electron spin configuration with $S = 1$. Splitting relative to the center of gravity at $g = 2.002$ is due to the presence of an electric (crystalline) field gradient

affecting the color centers through the spin-orbit interaction, characterized by the fine structure parameter (D) called zero-field splitting (ZFS). The mechanism responsible for phase inversion is associated with intercombination conversion during the optical transition from the ground 3A_2 to the excited state 3E . In this case, nonradiative recombination occurs through the intermediate metastable level 1A with the predominant population of the ground state with $M_S = 0$ (M_S is the quantum number of the electron spin projection). Thus, Boltzmann thermodynamic equilibrium, determined by the probability of population of each level with energy E_i by the factor $p_i = \exp(-E_i/k_B T)$, is violated. In this case, the high-field component of the fine structure represents an emission line, instead of absorbing microwave energy (unlike the low-field component).

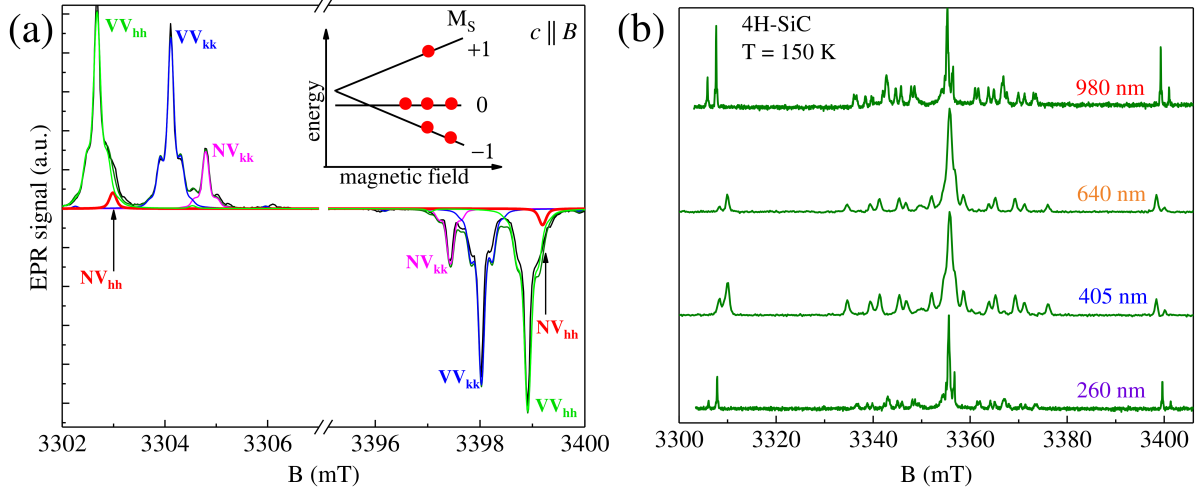


Figure 1. (a) W-band EPR spectrum of a 4H-SiC crystal in pulsed mode at $T = 150$ K under laser excitation with $\lambda = 532$ nm. Simulations for each center are highlighted in separate colors: VV_{hh} are green, VV_{kk} are blue, NV_{hh} are red and NV_{kk} are pink. The top inset shows the preferential occupancy of the state with $M_S = 0$ [22]; (b) Dependence of EPR spectra on laser wavelength [23].

To describe the EPR spectrum, a spin Hamiltonian with axial symmetry was used containing the components of electronic Zeeman splitting, fine structure, nuclear Zeeman splitting, and hyperfine (HFI) and nuclear quadrupole interaction (NQI) terms:

$$H = g\mu_B \mathbf{BS} + D \left(S_z^2 - \frac{1}{3} S(S+1) \right) + E (S_x^2 - S_y^2) - g_N \mu_N \mathbf{BI} + A_{\parallel} S_z I_z + A_{\perp} (S_x I_x + S_y I_y) + P \left(I_z^2 + \frac{1}{3} I(I+1) \right), \quad (1)$$

where g is the spectroscopic splitting factor, μ_B is the Bohr magneton, D (axial symmetry) and E (rhombohedral distortion) are the fine structure values, $S_{x,y,z}$ and $I_{x,y,z}$ are the projections of the electron and nuclear spin; A and P are the values of hyperfine and quadrupole interactions.

Thanks to the comparison of the data obtained with the results of previously published works on the study of a 4H-SiC crystal containing vacancy centers [5], the two divacancy (Table 1) and two nitrogen-vacancy NV^- (Table 2) centers were established. The registration of four signals of color centers is due to the presence of two structurally different positions of silicon and carbon atoms – hexagonal (h) and quasi-cubic (k) positions. Thus, in the EPR spectrum two axial NV_{kk} and NV_{hh} centers and two VV_{kk} and VV_{hh} divacancies directed along the crystallographic

Table 1. Spectroscopic values of the spin Hamiltonian for divacancies in a 4H-SiC crystal [24,25].

Color center	g	D (MHz)	E (MHz)
VV _{hh}	2.0033	1337	0
VV _{kk}	2.0041	1306	0
VV _{kh}	2.0038	1222	82
VV _{hk}	2.0035	1334.2	18.6

c -axis are observed. These color centers have approximately equal g -factor values, close to the value for a free electron ($g_e = 2.0023$). ZFS values for NV_{kk} $D = 1299.5$ MHz and for NV_{hh} $D = 1350$ MHz [22]. It is worth noting that the parameter E , which characterizes the orthorhombic distortion in the plane perpendicular to the c axis, is equal to zero and indicates the axial symmetry of the color centers observed in the EPR spectrum.

The D sign for NV[−] centers was established when the temperature was lowered to $T = 7$ K (Figure 2). At the indicated temperature, the value of $k_B T$ becomes comparable with the value of the photon $h\nu_{MW}$ ($\nu_{MW} = 94$ GHz), the difference in populations between the spin sublevels becomes significant and a redistribution of signal intensities occurs in the EPR spectrum. For the indicated conditions, the integrated intensity of the high-field component exceeded the same value for the low-field component, which corresponds to the positive sign of D [25]. In addition to the main correct simulation, the Figure 2 shows a low-temperature resonance MW absorption (dark green dots) of a spin defect with a negative D value. NV[−] centers in polytypes have the

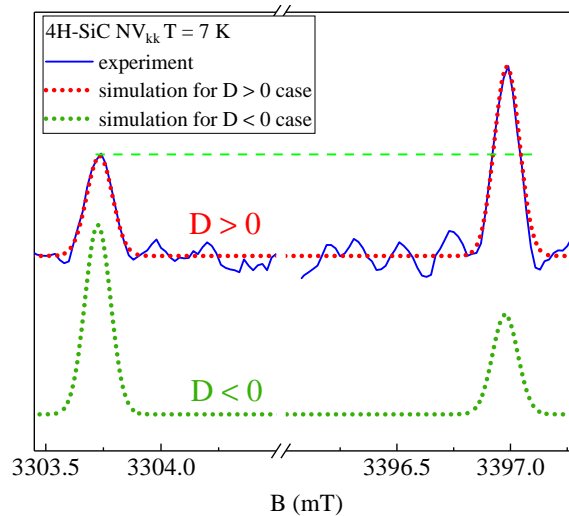


Figure 2. EPR spectrum of the NV_{kk} defect in a 4H-SiC crystal in the absence of laser excitation (dark spectrum recording). Blue solid line represents experimental values, red and dark green dots are simulations of the EPR spectra for positive and negative D values, respectively. EPR spectrum simulations were performed using EasySpin software in Matlab. The light green dashed line shows the difference in EPR intensities between the fine structure components. Adapted from [25].

same electronic structure with a triplet ground state 3A_2 and an excited state 3E . Measurements show that each type of NV[−] center is characterized by specific parameters of fine splitting (Table 2), hyperfine interaction and optical properties. In the ground state, the spin density is localized on the three neighboring C atoms of the Si vacancy, providing a strong hyperfine interaction with the ^{13}C nuclear spins [22]. The hyperfine interactions with the neighboring ^{14}N

and three neighboring ^{29}Si nuclei are small (≈ 1 MHz). Si atoms near the nearest neighbors of C atoms have higher hyperfine interaction constants (about 10 MHz), also resolved in the EPR spectra [13].

Table 2. Spectroscopic values of the spin Hamiltonian for NV^- centers for different configurations in SiC crystals [22, 26, 27].

Configuration	D (MHz)	E (MHz)
3C	1303	0
4H- kk	1282	0
4H- hh	1331	0
4H- hk	1193	110
4H- kh	1328	44
6H k_1k_2 (axial centers)	1355	0
6H hh (axial centers)	1328	0

3.2. Analysis of electron-nuclear interactions

To determine the parameters of hyperfine and quadrupole splittings caused by the presence of magnetic nuclei ^{14}N with $I = 1$, the ENDOR spectra recorded using the Mims pulse sequence were analyzed. Due to the interaction of electron spin $S = 1$ with nuclear magnetic and quadrupole moments, four additional nuclear magnetic resonance (NMR) transitions are formed according to the selection rule: $\Delta M_s = \pm 1$ and $\Delta m_I = \pm 1$ (m_I is the quantum number of the nuclear spin projection), according to the energy levels scheme on the Figure 3a (Adapted from [25]) for the low-field transition NV^- of the center. Figure 3b shows the ENDOR spectra for both transitions of the fine structure of color centers in parallel orientation of the crystal relative to the direction of the external magnetic field ($c \parallel B$). The ENDOR lines are localized near the Larmor frequency of the ^{14}N nucleus in accordance with the gyromagnetic ratio $\gamma = 3.077$ MHz/T and the value of $\mathbf{B} = 3.4$ T: $\nu_L = \gamma B = 10.2$ MHz. Thus, the ENDOR method makes it possible to establish the nature of the magnetic nuclei and the type of isotope (^{14}N) for the paramagnetic center under study.

To more accurately determine the values of hyperfine A and quadrupole P interactions, the angular dependencies of the position of absorption lines in the ENDOR spectrum (Figure 4) were measured when the crystal was rotated relative to the direction of the magnetic field \mathbf{B} :

$$\nu = |-g_N\mu_N B + m_s(a + b(3\cos^2\theta - 1)) + m_q P(3\cos^2\theta - 1)|/h, \quad (2)$$

where m_q is the average value of two nuclear spin manifolds between which NMR transitions are observed, θ is angle between the external magnetic field and the hexagonal axis of the crystal c .

Thanks to the appropriate simulation of experimental points using expression (2), the isotropic and anisotropic components of the hyperfine structure (a and b , respectively) were determined. The isotropic part a of the hyperfine interaction corresponds to the contribution of the contact Fermi interaction, which is determined by the value of the electron density of the color centers on the nitrogen nucleus ^{14}N [22]. The splitting of ENDOR lines due to this mechanism does not depend on the orientation of the crystal. The second important contribution to the magnitude of the hyperfine interaction is the anisotropic magnetic dipole-dipole interaction, which depends on the orientation of the crystal relative to the magnetic field as $3\cos^2\theta - 1$. The previously established sign of zero splitting D made it possible to determine the signs of the HFI values as

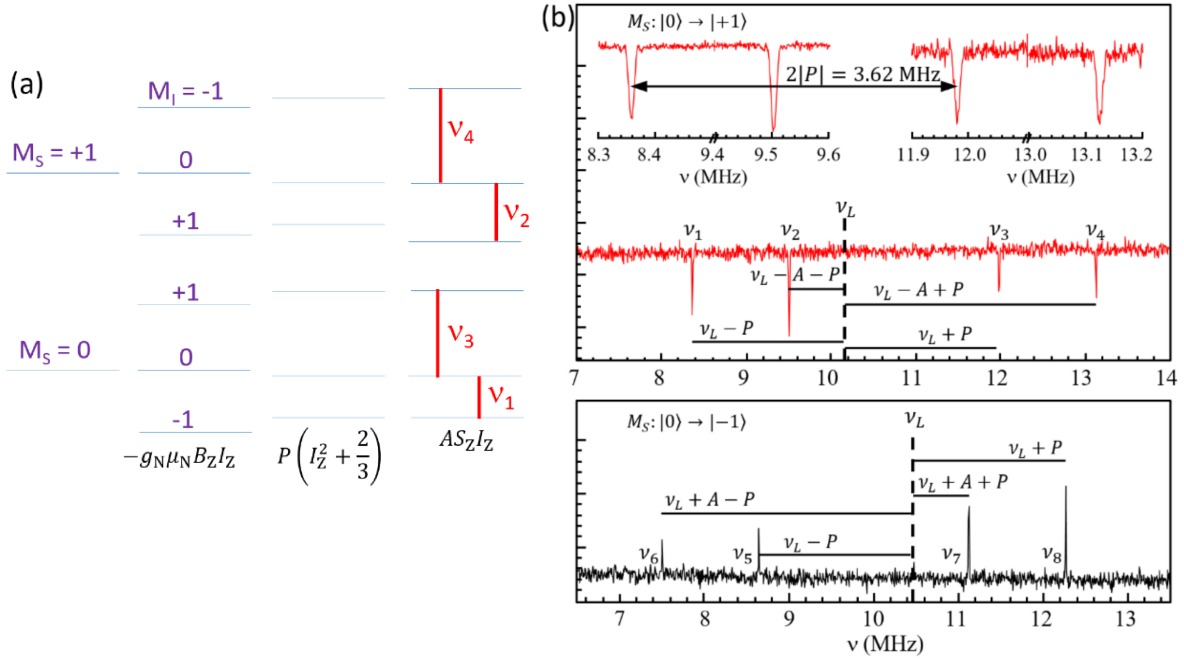


Figure 3. (a) NV^- levels diagram for low-field transition in accordance with the spin Hamiltonian (1), which contains electronic and nuclear Zeeman splitting, quadrupole and hyperfine interactions. Blue solid lines are electronic transitions with $\Delta M_s = \pm 1$ and $\Delta m_I = 0$, red solid lines are RF transitions of nuclear magnetic resonance with $\Delta M_s = \pm 1$ and $\Delta m_I = \pm 1$; (b) ENDOR spectra of a NV^- center in a 4H-SiC crystal: for the high-field (upper panel) and low-field (lower panel) components of the EPR spectrum; $c \parallel B$; $T = 150$ K [25].

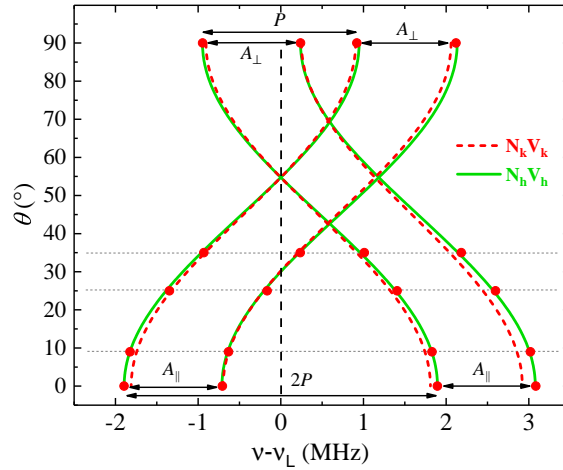


Figure 4. Angular dependence of the position of the ENDOR resonance lines for NV_{hh} (red dots are experimental, solid green lines are a simulation) and NV_{kk} (red dashed lines are a simulation, experimental values are not indicated for ease of visual perception). The experiments were carried out at temperature $T = 150$ K and laser excitation with $\lambda = 532$ nm [22].

negative for isotropic $a > 0$ and positive for dipole $b > 0$ deposits. Also, thanks to the simulation of the angular dependence of the ENDOR spectra, the magnitude and axial symmetry of the quadrupole interaction P were established. Spectroscopic values of electron-nuclear interactions are presented in Table 3. Thus, by determining the absolute values of the color center spin Hamiltonian constants, it is possible to establish the correct order of the electronic and nuclear spin sublevels.

Comparison of the experimental data obtained with theoretical calculations using the density functional theory method [25] allows us to confirm the microscopic model of the structure of color centers as the closest pair of a threefold coordinated silicon vacancy V_{Si} and an antisite N_C of nitrogen at the carbon position [22]. Thus, from the point of view of spectroscopic characteristics, the studied paramagnetic center is an analogue of nitrogen-vacancy color centers in diamond.

Table 3. Parameters of the spin Hamiltonian (1) for color centers in SiC extracted from the EPR and ENDOR spectra [13, 25–27].

Color center	$A_{ }$ (MHz)	a (MHz)	b (kHz)	P (MHz)
NV (3C)	1.26	−1.08	-	-
NV _{kk} (4H)	−1.142	−1.170	12	1.81
NV _{hh}	−1.165	−1.185	10	1.89
NV _{kh}	−0.970	−1.050	17	1.82
NV _{hk}	−0.650	−0.870	19	1.73
NV _{hh} (6H)	1.32	−1.08	-	-
NV _{k2k1}	1.21	−1.12	-	-
NV _{k1k2}	1.02	−1.02	-	-
NV _{k2k2}	1.00	−0.86	-	-
NV _{k1h}	0.67	−0.59	-	-
NV _{hk1}	1.00	−0.96	-	-

To study the dynamic characteristics of the NV^- centers, EPR experiments were carried out using standard Hahn sequences to record transverse relaxation times (T_2) and inversion-recovery curves to estimate longitudinal relaxation times (T_1). The measurements were carried out for the low-field component of the fine structure at $B \approx 3305$ mT. The value $T_1 = 0.5$ s was achieved when the temperature was lowered to $T = 7$ K. The maximum value of $T_2 = 49 \mu\text{s}$ was recorded at $T = 10$ K (with a further decrease in temperature T_2 doesn't change). For comparative analysis, T_2 was measured for divacancies (which don't have magnetic nuclei) and it turned out to be less: $T_2 = 40 \mu\text{s}$ [25]. A possible reason for this is that the electron spin density of the NV^- center is characterized by higher spatial localization than in the case of divacancy, which leads to less interaction of the electron spin NV^- with distant magnetic moments. The measured values are comparable with the electron relaxation times of centers NV^- in diamond [6].

4. Conclusion

Spin-Hamiltonian parameters for the NV^- centers in SiC in the ground electronic state using EPR and electron-nuclear double resonance spectroscopy were determined. Experimental data and its counterpart demonstrate that even slight differences in the local crystal structure may cause significant changes in the HFI and NQI values: the larger NQI value of the NV_{hh} defect with respect to NV_{kk} is due to a small shift of the ^{14}N atom away from the vacancy site. Although both basal and axial centers feature the substitutional nitrogen at the h site, the HFI of the latter is two times smaller.

The present results provide the crucial data for establishing protocols for transferring the electron spin polarization to the surrounding nuclear spins. The latter shows significant promise, particularly due to the recent successful generation of a single NV^- defect in SiC through ion implantation [28] and subsequent optical readout of the single NV^- defect spin [29]. Moreover,

these advancements are coupled with the theoretically predicted exceptionally long coherence times of these defects [30].

Acknowledgments

The study was funded by the subsidy allocated to Kazan Federal University for the state assignment in the sphere of scientific activities (Project No. FZSM-2024-0010).

References

1. Cao Y., Romero J., Olson J. P., Degroote M., Johnson P. D., Kieferová M., Kivlichan I. D., Menke T., Peropadre B., Sawaya N. P., Sim S., Veis L., Aspuru-Guzik A., *Chem. Rev.* **119**, 10856 (2019).
2. Tilley R. J., *Defects in Solids* (John Wiley & Sons, 2008) 552 p.
3. Ivády V., Abrikosov I. A., Gali A., *npj Comp. Mat.* **4**, 76 (2018).
4. Thiering G., Gali A., in *Semicond. and Semimetals*, Vol. 103, edited by Nebel C. E., Aharonovich I., Mizuochi N., Hatano M. (Elsevier, 2020) pp. 1–36.
5. Castelletto S., Boretti A., *J. Phys.: Photonics* **2**, 022001 (2020).
6. Awschalom D. D., Hanson R., Wrachtrup J., Zhou B. B., *Nature Photonics* **12**, 516 (2018).
7. Ruf M., Wan N. H., Choi H., Englund D., Hanson R., *J. Appl. Phys.* **130** (2021).
8. Rembold P., Oshnik N., Müller M. M., Montangero S., Calarco T., Neu E., *AVS Quant. Science* **2** (2020).
9. Du C., Van der Sar T., Zhou T. X., Upadhyaya P., Casola F., Zhang H., Onbasli M. C., Ross C. A., Walsworth R. L., Tserkovnyak Y., Yacoby A., *Science* **357**, 195 (2017).
10. Atatüre M., Englund D., Vamivakas N., Lee S.-Y., Wrachtrup J., *Nature Rev. Mater.* **3**, 38 (2018).
11. Soltamov V., Kasper C., Poshakinskiy A., Anisimov A., Mokhov E., Sperlich A., Tarasenko S., Baranov P., Astakhov G., Dyakonov V., *Nature Comm.* **10**, 1678 (2019).
12. Koehl W. F., Buckley B. B., Heremans F. J., Calusine G., Awschalom D. D., *Nature* **479**, 84 (2011).
13. von Bardeleben H. J., Cantin J. L., Csóré A., Gali A., Rauls E., Gerstmann U., *Phys. Rev. B* **94**, 121202 (2016).
14. Xu M., Girish Y. R., Rakesh K. P., Wu P., Manukumar H. M., Byrappa S. M., Byrappa K., *Material. Today Comm.* **28**, 102533 (2021).
15. Soltamov V. A., Yavkin B. V., Mamin G. V., Orlinskii S. B., Breev I. D., Bundakova A. P., Babunts R. A., Anisimov A. N., Baranov P. G., *Phys. Rev. B* **104**, 125205 (2021).
16. Yavkin B., Mamin G., Orlinskii S., *J. Magn. Res.* **262**, 15 (2016).
17. Yavkin B., Gafurov M., Volodin M., Mamin G., Orlinskii S. B., in *Experimental Methods in the Physical Sciences*, Vol. 50, edited by Shukla A. K. (Elsevier, 2019) pp. 83–113.

18. Wolfowicz G., Heremans F. J., Anderson C. P., Kanai S., Seo H., Gali A., Galli G., Awschalom D. D., *Nature Rev. Mater.* **6**, 906 (2021).
19. Cs  r   A., Von Bardeleben H. J., Cantin J.-L., Gali A., *Phys. Rev. B* **96**, 085204 (2017).
20. Vainer V., Il'in V., *Sov. Phys. Solid State* **23**, 2126 (1981).
21. Son N., Shafizadeh D., Ohshima T., Ivanov I., *J. Appl. Phys.* **132** (2022).
22. Murzakhanov F., Sadovnikova M., Mamin G., Nagalyuk S., von Bardeleben H. J., Schmidt W., Biktagirov T., Gerstmann U., Soltamov V., *J. Appl. Phys.* **134** (2023).
23. Murzakhanov F., *Vacancy centers in silicon carbide 4H-SiC and boron nitride hBN: electronic structure and spin polarization of triplet states*, PhD thesis in Physics and Mathematics (2023), 124 p., Kazan Federal University.
24. Magnusson B., Son N. T., Cs  r   A., G  llstr  m A., Ohshima T., Gali A., Ivanov I. G., *Phys. Rev. B* **98**, 195202 (2018).
25. Murzakhanov F., Yavkin B., Mamin G., Orlinskii S., von Bardeleben H. J., Biktagirov T., Gerstmann U., Soltamov V., *Phys. Rev. B* **103**, 245203 (2021).
26. Khazen K., von Bardeleben H. J., Zargaleh S. A., Cantin J.-L., Zhao M., Gao W., Biktagirov T., Gerstmann U., *Phys. Rev. B* **100**, 205202 (2019).
27. von Bardeleben H. J., Cantin J.-L., Gerstmann U., Schmidt W. G., Biktagirov T., *Nano Lett.* **21**, 8119 (2021).
28. Mu Z., Zargaleh S. A., von Bardeleben H. J., Froch J. E., Nonahal M., Cai H., Yang X., Yang J., Li X., Aharonovich I., Gao W., *Nano Lett.* **20**, 6142 (2020).
29. Wang J.-F., Yan F.-F., Li Q., Liu Z.-H., Liu H., Guo G.-P., Guo L.-P., Zhou X., Cui J.-M., Wang J., Zhou Z.-Q., Xu X.-Y., Xu J.-S., Li C.-F., Guo G.-C., *Phys. Rev. Lett.* **124**, 223601 (2020).
30. Zhu Y., Kovos B., Onizhuk M., Awschalom D., Galli G., *Phys. Rev. Mater.* **5**, 074602 (2021).